On the Use of a Lattice Model for Analyzing of In-Plane Vibration of Thin Plates

B. Šavija[1], E. Schlangen[1]

Abstract: In this paper, a novel approach for simulating in-plane vibration of thin plates is proposed. It is based on the spectral element method (SEM) used within a lattice modeling framework. First, derivation of a frequency dependent dynamic stiffness matrix for a spectral beam element is presented. Then, the lattice modeling concept is introduced. In the model, the two-dimensional plate is discretized as a set of (one dimensional) spectral beam elements connected at the ends. The proposed approach is then used for modal analysis of rectangular plates of different aspect ratios (1 and 2) and boundary conditions (completely free and clamped). Simulated natural frequencies and modal shapes are compared to results available in the literature. It was found that the proposed model can reasonably reproduce low natural frequencies (in most cases within 10%) and modal shapes. Future work will focus on the use of the model as an aid in non-destructive testing of structures.

1   Introduction

Spectral element method (SEM) has been used in recent years for dynamic analysis of structures [Doyle (1997)] as an alternative to the finite element method. It has shown to be suitable for modeling vibration of frame [Nefovska-Danilovic, Petronijevic and Šavija (2013)] and periodic structures [Lee (2009); Wu, Li and Zhang (2014)]. The SEM is a method for dynamic analysis which is based on elements whose stiffness matrices are obtained by solving the governing differential equations in the frequency domain. The element shape functions are based on the solution of the equation of motion, and, therefore, the displacement field within each element is an exact solution, and not an approximation. This is in contrast to the FEM, where usually polynomial shape functions are used to approximate the displacement field [Zienkiewicz and Taylor (2000)]. As a result, each geometrically and materially uniform structural element can be represented by a single spectral

---

[1] Microlab, Delft University of Technology, Delft, the Netherlands

element [Doyle (1997); Wu, Li and Zhang (2014)], greatly reducing the total number of elements in the analysis. In the SEM, the element shape functions (and element stiffness matrices) are frequency-dependent, and the analysis is performed in the frequency domain.

Lattice type models have been first used by theoretical physicists to model fracture mechanisms in heterogeneous materials [Moukarzel and Herrmann (1992)]. In such models, the material is discretized as a set of beam or truss elements, which transfer the load. This type of model has been adopted by various authors to simulate fracture in concrete (e.g. [Schlangen and van Mier (1992); Bolander and Saito (1998)]) and other anisotropic or heterogeneous materials (e.g. wood [Vasic, Smith and Landis (2005)] or porous reactor core graphite [Šavija, Liu, Smith, Hallam, Schlangen and Flewitt (2016)]. The use of lattice (or discrete) models has been further extended on simulating transport processes in porous materials such as concrete [Bolander and Berton (2004); Grassl (2009); Wang and Ueda (2011); Šavija, Pacheco and Schlangen (2013); Šavija, Luković and Schlangen (2014); Pacheco, Šavija, Schlangen and Polder (2014)], in which 1D "pipe" elements are used. In this work, an attempt is made to extend the lattice modeling concept to modeling dynamic behavior of structures by utilizing the SEM. This first effort is restricted to 2D analyses, and therefore the suitability of the proposed approach is assessed by analyzing in-plane vibrations of thin plates. Note, however, that the model proposed herein is different in nature compared to the model of Lee (1998), who used a continuum representation to simulate a periodic lattice structure: the model proposed herein uses a discrete representation of the continuum, in line with lattice approaches used for simulating fracture and transport.

Only a small number of publications have been devoted to in-plane vibration of plates. As the model proposed herein is two-dimensional, such works can be considered suitable for verification, Therefore, in this study, work of Bardell, Langley and Dunsdon (1996) is used as a reference to verify the proposed approach.

2 Modeling approach

2.1 Spectral elements

2.1.1 Spectral rod element

Partial differential equation of motion for a rod element is [Doyle (1997); Nefovska-Danilovic, Petronijevic and Šavija (2013)]:

$$EA\frac{\partial^2 u(x,t)}{\partial x^2} = \rho A\frac{\partial^2 u(x,t)}{\partial t^2} \tag{1}$$

Here, $u(x,t)$ is the longitudinal displacement, ρ the mass density, E Young's mod-

ulus, A the cross-sectional area, and t time.

Equation (1) can be solved by introducing a spectral representation of the displacement field [Doyle (1997); Nefovska-Danilovic, Petronijevic and Šavija (2013)]:

$$u(x,t) = U(x,\omega)e^{i\omega t} \tag{2}$$

where ω is the angular frequency. By inserting Eq. (2) in Eq. (1), the Fourier transform of Eq. (1) can be expressed as:

$$\frac{\partial^2 U}{\partial x^2} + k^2 U = 0 \tag{3}$$

where k is the wave number, with two possible values:

$$k_1^R = \sqrt{\omega^2 \left(\frac{\rho}{E}\right)} \tag{4}$$

$$k_2^R = -\sqrt{\omega^2 \left(\frac{\rho}{E}\right)} \tag{5}$$

The general solution of Eq. (3) can be written as:

$$U(x,\omega) = B_1 e^{ik_1^R x} + B_2 e^{ik_2^R x} \tag{6}$$

where B_1 and B_2 are constants which can be determined using boundary conditions at end nodes:

$$U(0) = U_1 \tag{7}$$
$$U(L) = U_2 \tag{8}$$

By combining Eq. (6) and Eqs. (7)–(8), the relationship between the vectors of nodal displacements $[U]$ and unknown constants can be written (in matrix form) as:

$$\begin{bmatrix} U_1 \\ U_2 \end{bmatrix} = [D_R] \begin{bmatrix} B_1 \\ B_2 \end{bmatrix} e^{i\omega t} \tag{9}$$

where $[D_R]$ is:

$$[D_R] = \begin{bmatrix} 1 & 1 \\ e^{ik_1^R L} & e^{ik_2^R L} \end{bmatrix} \tag{10}$$

Similarly, by utilizing the relation between axial force and strain:

$$f(x) = EA \frac{\partial U(x)}{\partial x} \tag{11}$$

the following matrix relation results:

$$\begin{bmatrix} F_1 \\ F_2 \end{bmatrix} e^{i\omega t} = [G_R] \begin{bmatrix} B_1 \\ B_2 \end{bmatrix} e^{i\omega t} \tag{12}$$

where $[G_R]$ is:

$$[G_R] = EA \begin{bmatrix} ik_1^R & ik_2^R \\ ik_1^R e^{ik_1^R L} & ik_2^R e^{ik_2^R L} \end{bmatrix} \tag{13}$$

The stiffness matrix relates the nodal displacements $[U_R]$ and nodal forces $[F_R]$:

$$[F_R] = [K_R][U_R] = [G_R][D_R]^{-1}[U_R] \tag{14}$$

The frequency dependent dynamic stiffness matrix for a rod element is given in as $[K_R] = [G_R][D_R]^{-1}$.

2.1.2   Spectral beam element

The dynamic stiffness matrix for a beam element can be derived in a similar manner as for the bar element. The equation of motion for an Euler-Bernoulli beam is:

$$EI\frac{\partial^4 w(x,t)}{\partial x^4} = -\rho A\frac{\partial^2 w(x,t)}{\partial t^2} \tag{15}$$

where $w(x,t)$ is the transverse displacement and I the moment of inertia.

Equation (15) can be solved by introducing a spectral representation of the transverse displacement field [Doyle (1997); Nefovska-Danilovic, Petronijevic and Šavija (2013)]:

$$w(x,t) = W(x,\omega)e^{i\omega t} \tag{16}$$

By combining Eqs. (16) and (15), the Fourier transform of Eq. (15) can be expressed as:

$$\frac{\partial^4 W}{\partial x^4} - k^4 W = 0 \tag{17}$$

where k is the wave number, with four possible values:

$$k_1^B = \sqrt[4]{\frac{\rho A\omega^2}{EI}} \tag{18}$$

$$k_2^B = i\sqrt[4]{\frac{\rho A\omega^2}{EI}} \tag{19}$$

$$k_3^B = -\sqrt[4]{\frac{\rho A \omega^2}{EI}} \tag{20}$$

$$k_4^B = -i\sqrt[4]{\frac{\rho A \omega^2}{EI}} \tag{21}$$

The general solution of Eq. (17) can be written as:

$$W(x,\omega) = C_1 e^{ik_1^B x} + C_2 e^{ik_2^B x} + C_3 e^{ik_3^B x} + C_4 e^{ik_4^B x} \tag{22}$$

where C_1–C_4 are constants which can be determined using boundary conditions at end nodes:

$$W(0) = W_1 \tag{23}$$
$$\Psi(0) = \Psi_1 \tag{24}$$
$$W(L) = W_2 \tag{25}$$
$$\Psi(L) = \Psi_2 \tag{26}$$

where Ψ is the rotation (see Fig. 1). By combining Eq. (22) and Eqs. (23)–(26), and keeping in mind that $\Psi = \frac{\partial w}{\partial x}$, the relationship between the vector of nodal displacements $[U_B]$ and unknown constants can be written as (in matrix form):

$$\begin{bmatrix} W_1 \\ \Psi_1 \\ W_2 \\ \Psi_2 \end{bmatrix} = [D_B] \begin{bmatrix} C_1 \\ C_2 \\ C_3 \\ C_4 \end{bmatrix} e^{i\omega t} \tag{27}$$

where $[D_B]$ matrix for a beam element is:

$$[D_B] = \begin{bmatrix} 1 & 1 & 1 & 1 \\ ik_1^B & ik_2^B & ik_3^B & ik_4^B \\ e^{ik_1^B L} & e^{ik_2^B L} & e^{ik_3^B L} & e^{ik_4^B L} \\ ik_1^B e^{ik_1^B L} & ik_2^B e^{ik_2^B L} & ik_3^B e^{ik_3^B L} & ik_4^B e^{ik_4^B L} \end{bmatrix} \tag{28}$$

By utilizing the relation between vertical displacements and node forces:

$$EI\left(\frac{\partial^3 W}{\partial x^3}\right)_0 = F_{y1} \tag{29}$$

$$-EI\left(\frac{\partial^2 W}{\partial x^2}\right)_0 = M_1 \tag{30}$$

$$-EI\left(\frac{\partial^3 W}{\partial x^3}\right)_L = F_{y2} \tag{31}$$

$$EI \left(\frac{\partial^2 W}{\partial x^2} \right)_L = M_2 \tag{32}$$

the following matrix relation results:

$$\begin{bmatrix} F_{y1} \\ M_1 \\ F_{y2} \\ M_2 \end{bmatrix} e^{i\omega t} = [G_B] \begin{bmatrix} B_1 \\ B_2 \\ B_3 \\ B_4 \end{bmatrix} e^{i\omega t} \tag{33}$$

where $[G_B]$ is:

$$[G_B] = \begin{bmatrix} -i(k_1^B)^3 & -i(k_2^B)^3 & -i(k_3^B)^3 & -i(k_4^B)^3 \\ (k_1^B)^2 & (k_2^B)^2 & (k_3^B)^2 & (k_4^B)^2 \\ i(k_1^B)^3 e^{ik_1^B L} & i(k_2^B)^3 e^{ik_2^B L} & i(k_3^B)^3 e^{ik_3^B L} & i(k_4^B)^3 e^{ik_4^B L} \\ -(k_1^B)^2 e^{ik_1^B L} & -(k_2^B)^2 e^{ik_2^B L} & -(k_3^B)^2 e^{ik_3^B L} & -(k_4^B)^2 e^{ik_4^B L} \end{bmatrix} \tag{34}$$

The stiffness matrix relates the nodal displacements $[U_B]$ and nodal forces $[F_B]$:

$$[F_B] = [K_B][U_B] = [G_B][D_B]^{-1}[U_B] \tag{35}$$

The frequency dependent dynamic stiffness matrix for a beam element is given as $[K_B] = [G_B][D_B]^{-1}$.

2.1.3   Spectral element

The dynamic stiffness matrix for a two-dimensional element comprises both stiffness matrices for a rod and for bending, as previously derived. The relation between the spectral nodal displacements and forces can be expressed in the matrix form as [Doyle (1997); Nefovska-Danilovic, Petronijevic and Šavija (2013); Wu, Li and Zhang (2014)]:

$$K(\omega)q = F \tag{36}$$

where $K(\omega)$ is the dynamic stiffness matrix, $q = [U_1 \quad W_1 \quad \Psi_1 \quad U_2 \quad W_2 \quad \Psi_2]^T$ the vector of (all) nodal displacements, and $F = [F_{x1} \quad F_{y1} \quad M_1 \quad F_{x2} \quad F_{y2} \quad M_2]^T$ the vector of (all) nodal forces (see figure 1). The element stiffness matrix is frequency dependent of the following form:

$$K(\omega) = \begin{bmatrix} K_{11}^R & 0 & 0 & K_{12}^R & 0 & 0 \\ 0 & K_{11}^B & K_{12}^B & 0 & K_{13}^B & K_{14}^B \\ 0 & K_{21}^B & K_{22}^B & 0 & K_{23}^B & K_{24}^B \\ K_{21}^R & 0 & 0 & K_{22}^R & 0 & 0 \\ 0 & K_{31}^B & K_{32}^B & 0 & K_{33}^B & K_{34}^B \\ 0 & K_{41}^B & K_{42}^B & 0 & K_{43}^B & K_{44}^B \end{bmatrix} \tag{37}$$
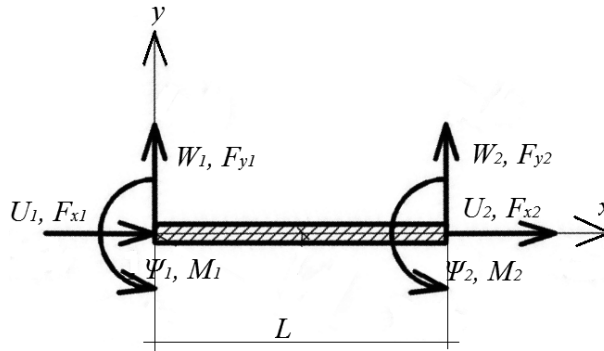
Figure 1: A beam element in a local coordinate system

In Eq. (37), the superscripts *R* and *B* refer to rod and beam, respectively. Subscripts denote the position of each entry in the dynamic stiffness matrix of a rod or a beam. A typical beam element in the local coordinate system is shown in Fig. 1. It can be seen that axial and bending motion are decoupled. The dynamic stiffness matrix in the global coordinate system for a structure is further obtained by using transformation and assembling procedure, the same as in the FEM [Zienkiewicz and Taylor (2000)].

2.2   *Lattice modeling concept*

In the lattice model as used herein, the material is discretized as a set of spectral beam elements (Fig. 2). Therefore, the plate is modeled using simple beam elements with three degrees of freedom per node, two translations and one rotation (see Fig. 1). The plate is divided into a number of quadratic cells with a unit length of *h*, and a node is placed within each of these cells. These are the end nodes of lattice beam elements. A regular quadrangular lattice is used, connecting nodes in neighboring cells. Cross sectional area and moment of inertia of each beam element are defined as:

$$A = hd \tag{38}$$
$$I = 1/12h^3d \tag{39}$$

where *d* is the out-of plane thickness of the analyzed plate. The volume of the plate needs also to be converted to the volume of the equivalent lattice. It needs to be noted that, in this procedure, a certain overlap exists between neighboring lattice elements (Fig. 3). Therefore, in the calculation of the stiffness matrix of the spectral beam, the mass density (ρ) is divided by a correction factor η, which is defined as [Nakamura, Srisoros, Yashiro and Kunieda (2006)]:
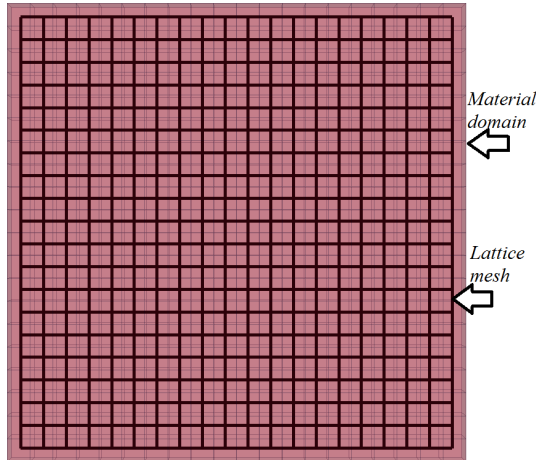
Figure 2: Discretization of the material domain by a lattice mesh
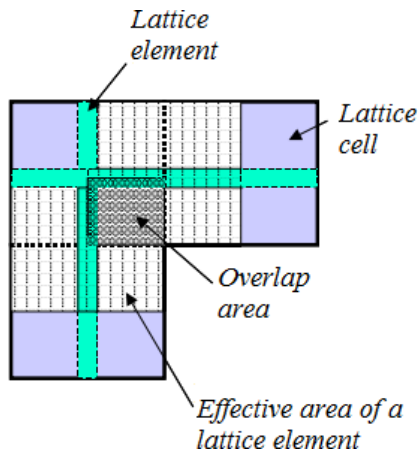
Figure 3: Definition of overlap area for determination of parameter η [Nakamura, Srisoros, Yashiro and Kunieda (2006)]

$$\eta = \frac{\sum_{k=1}^{n} A_k L_k}{V} \tag{40}$$

where n is the total number of lattice elements, A_k the cross-sectional area of each lattice element, L_k the length of each lattice element, i the element number, and V the total volume of the plate. The correction factor η, therefore, ensures that the total mass of the plate is conserved after the lattice discretization. Note that in an infinite square lattice, $\eta = 2$, while in a finite rectangular lattice, η is somewhat lower, due to the effect of the domain boundaries.

3   Validation and discussion

In their work, Bardell, Langley and Dunsdon (1996) used the Rayleigh-Ritz method to study in-plane vibration of isotropic rectangular plates with varying boundary conditions. Apart from the modal frequencies, modal shapes for different test cases are provided. As the methodology presented in the current paper is quite new, it is necessary to test both the accuracy of the simple lattice model in terms of natural frequencies and its ability to reproduce correct modes of vibration. Therefore, work of Bardell, Langley and Dunsdon (1996) was selected as a benchmark for evaluation of the proposed model.

The modal frequencies can be determined as angular frequencies ω for which the following is true:

$$det(K(\omega)) = 0 \tag{41}$$

The proposed model was used to analyze two rectangular plates with aspect ratios of $a/b = 1$ and $a/b = 2$. The material properties used in the calculation were $E = 207$ GPa, $\rho = 7800$ kg/m^3 and $v = 0.3$. A lattice cell of a unit cell size ($h = 1$) was used in all analyses. The calculated natural frequencies were transformed into a non-dimensional form by using the following equation:

$$\Omega = \frac{\omega a}{C_L} \tag{42}$$

where C_L is the longitudinal wave speed:

$$C_L = \sqrt{\frac{E}{\rho(1 - v^2)}} \tag{43}$$

and compared to those obtained by Bardell, Langley and Dunsdon (1996). Furthermore, the mode shapes were plotted and compared as well.

The first analyzed case was a completely free square plate (i.e. with an aspect ratio of $a/b = 1$) with $a = 10h$. The first five vibration modes and natural frequencies are shown in Fig. 4.

It is interesting to note that modes 1–3 correspond to modes by Bardell, Langley and Dunsdon (1996), while mode 4 corresponds to mode 5, and mode 5 to mode 4. In Fig. 5, a comparison between the non-dimensional natural frequencies calculated using the simple lattice model and those provided by Bardell, Langley and Dunsdon (1996) is given. The proposed model predicts somewhat higher values of natural frequencies than the benchmark results. Given the simplicity of the model, it can be said that reliable results are obtained for lower modes of vibration.
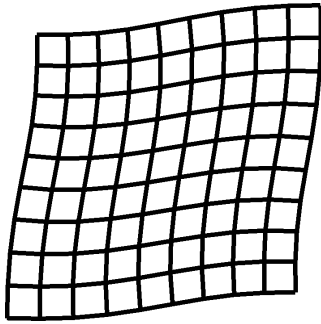
(a) Mode 1, $\Omega_1 = 2.413$ (*Mode 1, $\Omega_{1B} = 2.321$*)
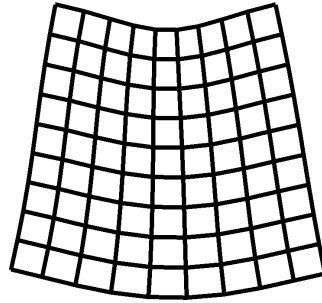
(b) Mode 2, $\Omega_2 = 2.775$ (*Mode 2, $\Omega_{2B} = 2.472$*)
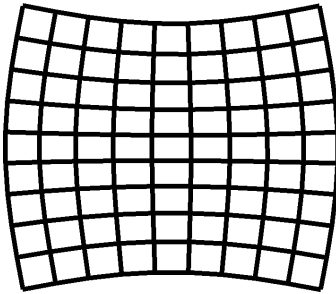
(c) Mode 3, $\Omega_3 = 3.016$ (*Mode 3, $\Omega_{3B} = 2.628$*)
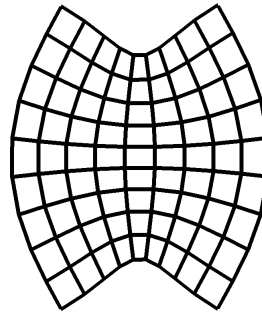
(d) Mode 4, $\Omega_4 = 3.079$ (*Mode 5, $\Omega_{5B} = 3.452$*)
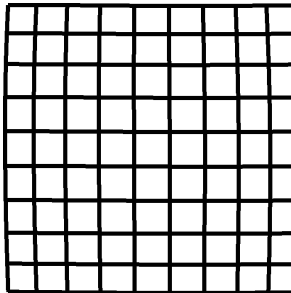
(e) Mode 5, $\Omega_5 = 3.445$ (*Mode 4, $\Omega_{4B} = 2.987$*)

Figure 4: Modes and natural frequencies of a free isotropic plate, $a = b$. In parentheses, the corresponding mode and natural frequency reported by Bardell, Langley and Dunsdon (1996) is given

The second case analyzed was a completely free rectangular plate with an aspect ratio of $a/b = 2$ with $a = 20h$. The first six vibration modes and natural frequencies are shown in Fig. 6.
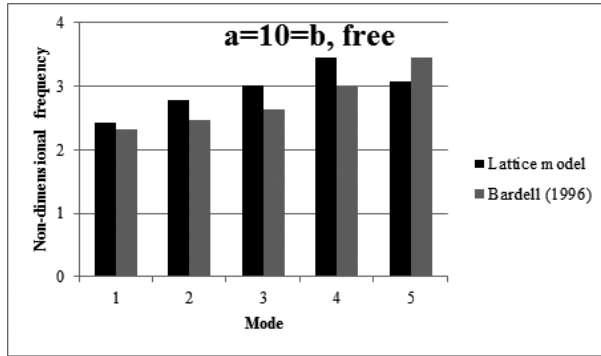
Figure 5: Comparison between natural frequencies calculated by the lattice model, and the benchmark results [Bardell, Langley and Dunsdon (1996)], for a free isotropic plate, $a = b$
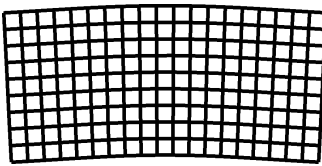
(a) Mode 1, $\Omega_1 = 1.995$ (*Mode 1, $\Omega_{1B} = 1.954$*)
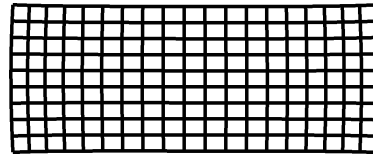
(b) Mode 2, $\Omega_2 = 2.885$ (*Mode 2, $\Omega_{2B} = 2.961$*)
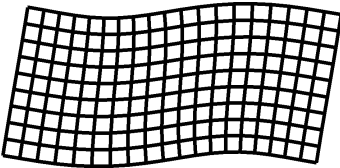
(c) Mode 3, $\Omega_3 = 3.498$ (*Mode 3, $\Omega_{3B} = 3.267$*)
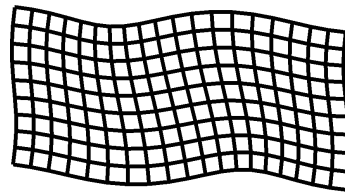
(d) Mode 4, $\Omega_4 = 5.107$ (*Mode 4, $\Omega_{4B} = 4.726$*)
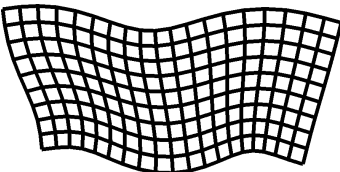
(e) Mode 5, $\Omega_5 = 5.140$ (*Mode 5, $\Omega_{5B} = 4.784$*)
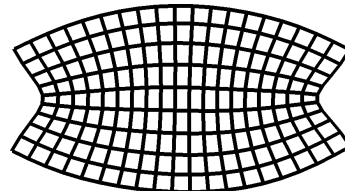
(f) Mode 6, $\Omega_6 = 6.146$ (*Mode 6, $\Omega_{6B} = 5.205$*)

Figure 6: Modes and natural frequencies of a free isotropic plate, $a = 2b$. In parentheses, the corresponding mode and natural frequency reported by Bardell, Langley and Dunsdon (1996) is given
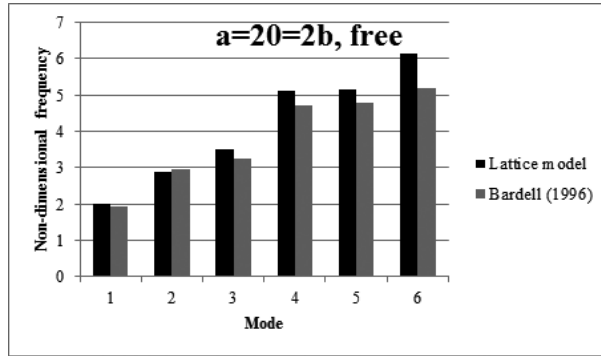
Figure 7: Comparison between natural frequencies calculated by the lattice model, and the benchmark results [Bardell, Langley and Dunsdon (1996)], for a free isotropic plate, $a = 2b$
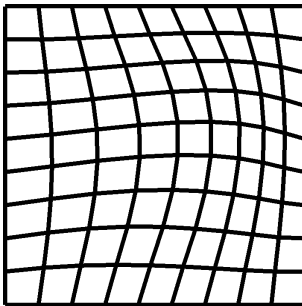
(a) Mode 1, $\Omega_1 = 3.508$ (*Mode 1, $\Omega_{1B} = 3.555$*)
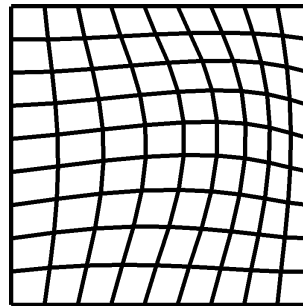
(b) Mode 2, $\Omega_2 = 4.859$ (*Mode 2, $\Omega_{2B} = 4.235$*)
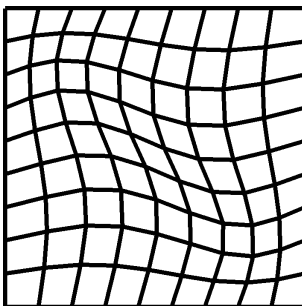
(c) Mode 3, $\Omega_3 = 5.351$ (*Mode 3, $\Omega_{3B} = 5.186$*)
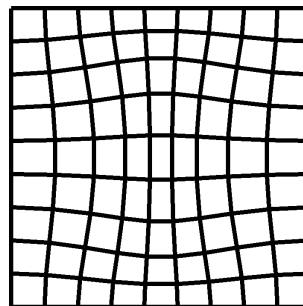
(d) Mode 4, $\Omega_4 = 5.696$ (*Mode 4, $\Omega_{4B} = 5.859$*)

Figure 8: Modes and natural frequencies of a clamped isotropic plate, $a = b$. In parentheses, the corresponding mode and natural frequency reported by Bardell, Langley and Dunsdon (1996) is given

In this case, all predicted vibration modes correspond to those reported by Bardell, Langley and Dunsdon (1996). Comparison between the calculated natural frequencies and the benchmark values for this case is given in Fig. 11. It can be noticed that in this case, too, the model shows a small overestimation of natural frequencies.

The third analyzed case was a square plate ($a/b = 1$) with all its edges clamped, with $a = 10h$. These boundary conditions in the lattice analysis were applied as full constraint (i.e. both displacements and rotation) at lattice edge nodes. The first four vibration modes and natural frequencies are shown in Fig. 8.

Bardell, Langley and Dunsdon (1996) reported the first five natural frequencies and modes for this analysis case. In the simple lattice analysis herein, however, mode 5 was not detected. The first four modes of vibration correspond to the benchmark case. The deviation between the calculated natural frequencies and the benchmark values is small, and is shown in Fig. 9.
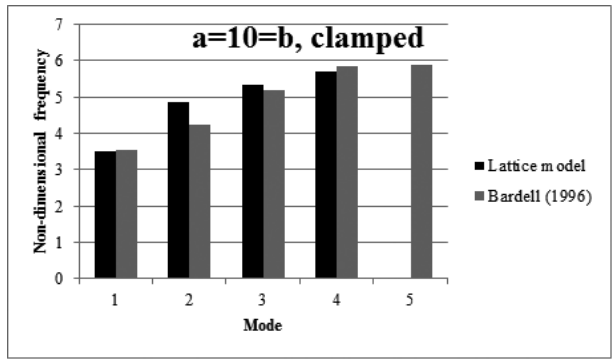
Figure 9: Comparison between natural frequencies calculated by the lattice model, and the benchmark results [Bardell, Langley and Dunsdon (1996)], for a clamped isotropic plate, $a = b$

The last case analyzed was a rectangular plate with all its edges clamped, with an aspect ratio of $a/b = 2$ with $a = 20h$. The same as in the previous case, full constraints were applied at the edge nodes of the lattice. The first five vibration modes observed and their natural frequencies are shown in Fig. 10.

The lattice model predicts the first three vibration modes very well. However, mode 4 from the benchmark was not predicted (note the caption in Fig. 10). Modes 5 and 6 were also predicted well. A comparison between the natural frequencies from the lattice model and the benchmark values is given in Fig. 11. Same as in other analysis cases, there is a small deviation between the natural frequencies.

(a) Mode 1, $\Omega_1 = 1.995$ (*Mode 1,* $\Omega_{1B} = 1.954$)

(b) Mode 2, $\Omega_2 = 2.885$ (*Mode 2,* $\Omega_{2B} = 2.961$)

(c) Mode 3, $\Omega_3 = 3.498$ (*Mode 3,* $\Omega_{3B} = 3.267$)

(d) Mode 4, $\Omega_4 = 5.107$ (*Mode 4,* $\Omega_{4B} = 4.726$)

(e) Mode 5, $\Omega_5 = 5.140$ (*Mode 5,* $\Omega_{5B} = 4.784$)
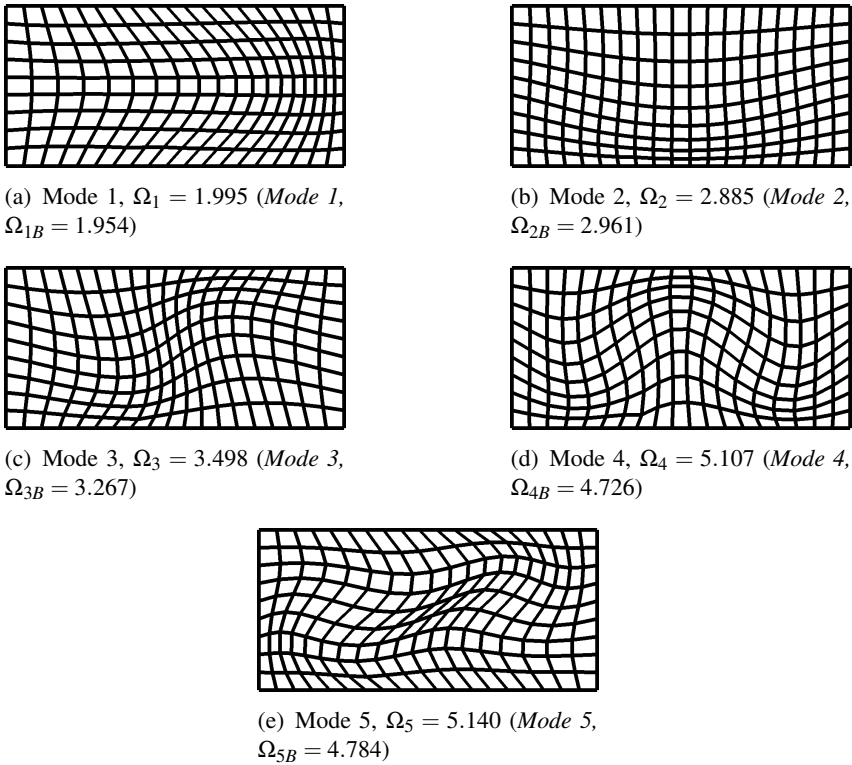
Figure 10: Modes and natural frequencies of a clamped isotropic plate, $a = 2b$. In parentheses, the corresponding mode and natural frequency reported by Bardell, Langley and Dunsdon (1996) is given
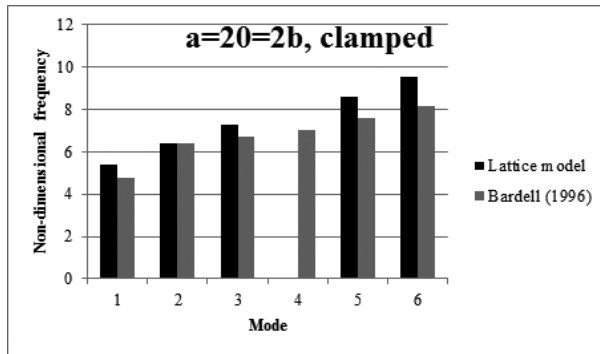
Figure 11: Comparison between natural frequencies calculated by the lattice model, and the benchmark results [Bardell, Langley and Dunsdon (1996)], for a clamped isotropic plate, $a = 2b$

In order to check if there is an effect of mesh size on the calculated natural frequencies, the first analysis (free square plate, $a = b$) was repeated for two other mesh sizes: $a = 5h$, and $a = 20h$. The analysis results (together with the analysis with $a = 10h$ and the benchmark results) are given in Fig. 12.
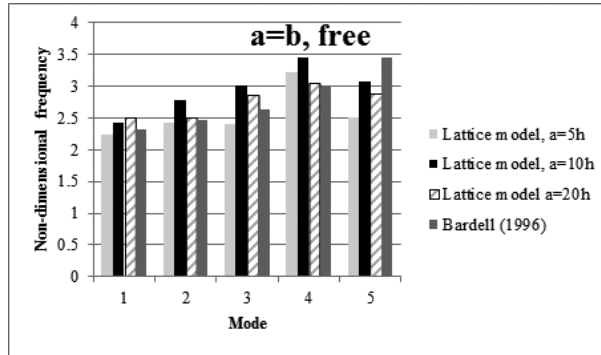
Figure 12: Comparison between natural frequencies calculated by the lattice model of different mesh size, and the benchmark results Bardell, Langley and Dunsdon (1996), for a free isotropic plate, $a = b$

All three mesh sizes predict natural frequencies close to the benchmark results. Even though some differences between the three meshes were observed, there were no clear improvements resulting from the increased mesh size (or mesh density).

The proposed model is able to reliably calculate the natural frequencies and modal shapes for in-plane vibrations of thin plates for low vibration modes. The error between the simulated results and the benchmark is mainly less than 10%, which can be considered good when the simple nature of the model is taken into account. Some of the deviation could be probably ascribed to the use of such simple square lattice grid of beams. Such a lattice cannot reproduce the Poisson's ratio of the continuum, as its global Poisson's ratio is equal to zero. Similar limitations apply also to triangular 2D lattice arrangements, which can (under uniform strain) reproduce global Poisson's ratio of $-1 < v < 1/3$ [Schlangen and Garboczi (1997)]. Some of the recent approaches were able to overcome this issue (albeit in a 3D lattice arrangement) [Jivkov and Yates (2012)]. In the two examples dealing with the constrained mesh boundaries, another issue was that some of the vibration modes were not observed using the lattice modeling approach. Another source of this could be the manner in which the boundary conditions are applied in the lattice model: only lattice nodes were constrained, while the beams were free between the nodes. This is somewhat different compared to other methods. Combined with the issue of the global Poisson's ratio, it is a possible source of deviation.

It is recognized that there are possibilities of using other methods for modeling

in-plane vibration of thin plates, even with a higher precision. Besides the FEM, spectral plate elements were recently presented with such capabilities [Nefovska-Danilovic and Petronijevic (2015); Kolarevic, Nefovska-Danilovic and Petronijevic (2015); Kolarevic, Marjanović, Nefovska-Danilovic and Petronijevic (2016)]. Other methods for simulating microcracking in heterogeneous composites [Dong and Atluri (2013); Dong, Alotaibi, Mohiuddine and Atluri (2014)] are also available. However, besides its relative simplicity, the proposed lattice method has several advantages. It can be further extended on studying modal characteristics and vibration of cracked heterogeneous solids, such as concrete. First, the fracture simulation would be performed using the fracture lattice model [Schlangen and Qian (2009)]. In the fracture lattice model, cracks are simulated by removing "cracked" beams from the lattice mesh. Following the fracture analysis, using the cracked configuration as input, modal analysis would be performed. As it is known that any change in natural frequency can be a sign of structural damage [Salawu (1997)], such model could be used as aid in non-destructive testing of structures. It is further envisioned that such a method could be useful in studying recovery of modal properties due to repair and self-healing of concrete structures [de Rooij, Van Tittelboom, De Belie and Schlangen (2013); Tzviloglou, Van Tittelboom, Palin, Wang, Sierra-Beltrán, Erşan, Mors, Wiktor, Jonkers, Schlangen et al. (2016)]. Similar efforts in combining discrete models with non-destructive testing of deterioration are already under development [Alnaggar, Cusatis, Qu and Liu (2014)]. A simple example of such application of the model is given next.

4   Example of application

In this section, the developed model is applied for modal analysis of a slice of a simply supported concrete beam (160x40x1mm^3). The beam consists of spherical inclusion (aggregate) particles embedded in a mortar matrix. The model was first subjected to a simulated three-point bending test, using the Delft lattice model [Schlangen and Qian (2009)]. In the model, all individual elements exhibit linear elastic behavior. The fracture simulation is achieved by performing a linear elastic analysis of the lattice under loading, and removing an element which exceeds a prescribed fracture criterion (e.g. strength, strain, or energy) from the mesh. This analysis is then repeated in a step-wise manner, removing a single element in each-step. Thus, a non-linear analysis is performed by actually performing a number of linear analyses. Using this method, realistic crack patterns are found. Furthermore, even though individual elements all behave brittle, a ductile global response is achieved [Schlangen and Qian (2009)]. Mechanical properties used in the analysis are given in table 1. The simulated load-displacement curve is shown in figure 13.

Table 1: Mechanical properties used in the analysis

Phase	E modulus (*GPa*)	Tensile strength (*MPa*)	Density (kg/m^3)
Mortar	20	4	2100
Aggregate	70	8	2600
Interface	15	2.5	2100
Glue	3.5	20	1060
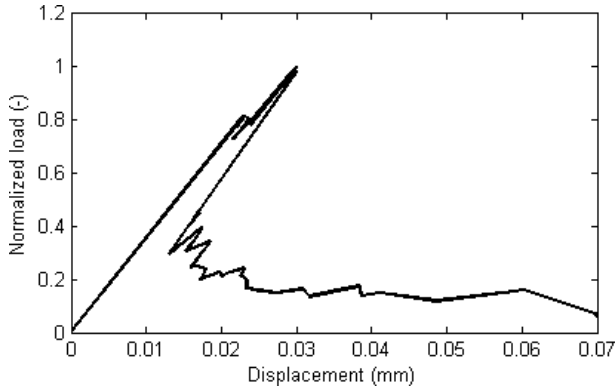
Figure 13: Load-displacement curve for the three-point bending simulation

Natural frequencies were calculated for different stages in the cracking process: initial mesh, at peak load, and at failure (See figure 13). For the crack states, "crack" elements were removed from the mesh prior to modal analysis. Then, the natural frequencies of the cracked specimen are compared to the initial values (Table 2). The cracks are assumed to be repaired/healed using glue (i.e. cracked elements are replaced by glue elements), which is a promising mechanism for self-healing of concrete [Feiteira, Gruyaert and De Belie (2016)]. Modal analysis is performed again, and the recovery of natural frequencies is observed.

Table 2: Calculated natural frequencies for all analyses (Hz)

	Initial	Cracked (peak)	Cracked (pre-failure)	Repaired/healed
Mode 1	86	85	67	84
Mode 2	112	112	106	112
Mode 3	202	202	146	202

Microcracks occurring prior to the peak load (Figure 14b) cause a very small decrease in the first natural frequency. Second and third mode are not affected. This is also related to the damage location, because here the stiffness loss is in the mid-

(a) Material structure showing matrix (black), aggregates (brown) and the interface (light brown)

(b) Cracks at peak load

(c) Cracks prior to failure

(d) Repaired/healed cracks
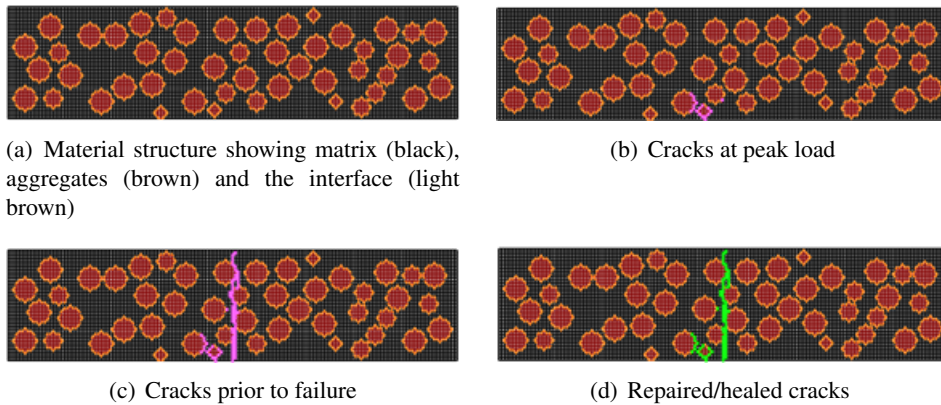
Figure 14: Fracture simulation and assumed healing/repairing of broken lattice elements (b, c-pink -cracks; green -repaired/healed elements)

dle of the span, which causes a reduction in mode 1 [Salawu (1997)]. Just prior to failure (Figure 14c), the first three modes are all significantly reduced, indicating significant damage. After the healing event (assuming complete filling of all cracks with glue), the natural frequencies have recovered, except the first natural frequency, which is still somewhat lower compared to the initial one. The reason for this is that, although the glue has filled up the crack, it has a somewhat lower stiffness compared to the initial material (see Table 1). Due to the modal shape of mode 1, this mode is particularly affected by loss of stiffness in the middle of the beam span.

From this simple example, it can be concluded that the model is able to detect changes in natural frequencies caused by cracking, and their subsequent recovery after crack healing. However, the model cannot be used in a quantitative sense due to its 2D nature, and needs to be extended to 3D and further validated.

5 Conclusions

In this paper, a simple model for in-plane vibration of thin plates is presented. Based on the spectral element method (SEM), and using the lattice modeling principle, it can be seen as an alternative to other methods, such as the FEM. The 2D plate is discretized as a set of spectral beam elements connected at the nodes. The stiffness matrix of a spectral beam element is frequency dependent, and the analysis is performed in the frequency domain. In this paper, the proposed approach is tested and verified for modal analysis of in-plane vibrations of rectangular plates. The validation procedure has lead to the following conclusions:

- The lattice model provides reliable results for natural frequencies of the plates, mainly within less than 10% error for lower vibration modes in analyzed cases.

- In case of completely free plates, all the vibration modes were correctly reproduced by the model. Only in case of a square plate, two higher modes (mode 4 and mode 5) were permuted compared to the benchmark results of Bardell, Langley and Dunsdon (1996).

- In case of clamped plates, most vibration modes were correctly reproduced by the model. However, for both analyzed plates (i.e. with aspect ratios of $a/b = 1$ and $a/b = 2$), one of the first five vibration modes was not detected by the model (mode 5 and mode 4 for $a/b = 1$ and $a/b = 2$, respectively). This can probably (at least in part) be attributed to the the way that boundary conditions are applied in the lattice model.

- Mesh size seems not to have a large effect on the calculated natural modes. This was expected, as in the SEM the mass is distributed over the length of the beam, and not lumped in the nodes.

Finally, a simple example of modal analysis of cracked and healed concrete is given. The example showed that, in general, the model is able to reproduce a shift in natural frequencies due to cracking and healing. This needs to be explored and validated, and will be a subject of further study. Once validated, the model will provide a valuable tool in assisting to non-destructive testing of cracked and repaired/healed structures.

References

Alnaggar, M.; Cusatis, G.; Qu, J.; Liu, M. (2014): Simulating acoustic non-linearity change in accelerated mortar bar tests: A discrete meso-scale approach. In Furuta, H.; Frangopol, D.; Akiyama, M.(Eds): *Life-cycle of structural systems: design, assessment, maintenance and management*, pp. 451–458. CRC Press.

Bardell, N.; Langley, R.; Dunsdon, J. (1996): On the free in-plane vibration of isotropic rectangular plates. *Journal of Sound and Vibration*, vol. 191, no. 3, pp. 459–467.

Bolander, J.; Berton, S. (2004):   Simulation of shrinkage induced cracking in cement composite overlays. *Cement and Concrete Composites*, vol. 26, no. 7, pp. 861–871.

Bolander, J.; Saito, S. (1998):   Fracture analyses using spring networks with random geometry. *Engineering Fracture Mechanics*, vol. 61, no. 5, pp. 569–591.

de Rooij, M.; Van Tittelboom, K.; De Belie, N.; Schlangen, E. (2013): *Self-Healing Phenomena in Cement-Based Materials: State-of-the-Art Report of RILEM Technical Committee 221-SHC: Self-Healing Phenomena in Cement-Based Materials*, volume 11. Springer.

Dong, L.; Alotaibi, A.; Mohiuddine, S.; Atluri, S. (2014):   Computational methods in engineering: a variety of primal & mixed methods, with global & local interpolations, for well-posed or ill-posed bcs. *CMES: Computer Modeling in Engineering & Sciences*, vol. 99, no. 1, pp. 1–85.

Dong, L.; Atluri, S. N. (2013):   Sgbem voronoi cells (svcs), with embedded arbitrary-shaped inclusions, voids, and/or cracks, for micromechanical modeling of heterogeneous materials. *CMC: Computers, Materials & Continua*, vol. 33, no. 2, pp. 111–154.

Doyle, J. F. (1997):   *Wave propagation in structures: Spectral analysis using fast discrete Fourier transforms.* Springer.

Feiteira, J.; Gruyaert, E.; De Belie, N. (2016):   Self-healing of moving cracks in concrete by means of encapsulated polymer precursors. *Construction and Building Materials*, vol. 102, pp. 671–678.

Grassl, P. (2009):   A lattice approach to model flow in cracked concrete. *Cement and Concrete Composites*, vol. 31, no. 7, pp. 454–460.

Jivkov, A. P.; Yates, J. R. (2012):   Elastic behaviour of a regular lattice for meso-scale modelling of solids. *International Journal of Solids and Structures*, vol. 49, no. 22, pp. 3089–3099.

Kolarevic, N.; Marjanović, M.; Nefovska-Danilovic, M.; Petronijevic, M. (2016):   Free vibration analysis of plate assemblies using the dynamic stiffness method based on the higher order shear deformation theory. *Journal of Sound and Vibration*, vol. 364, pp. 110–132.

Kolarevic, N.; Nefovska-Danilovic, M.; Petronijevic, M. (2015):   Dynamic stiffness elements for free vibration analysis of rectangular mindlin plate assemblies. *Journal of Sound and Vibration*, vol. 359, pp. 84–106.

Lee, U. (1998):   Equivalent continuum representation of lattice beams: spectral element approach. *Engineering Structures*, vol. 20, no. 7, pp. 587–592.

Lee, U. (2009):   *Spectral element method in structural dynamics*. John Wiley & Sons.

Moukarzel, C.; Herrmann, H. (1992):   A vectorizable random lattice. *Journal of Statistical Physics*, vol. 68, no. 5-6, pp. 911–923.

Nakamura, H.; Srisoros, W.; Yashiro, R.; Kunieda, M. (2006):   Time-dependent structural analysis considering mass transfer to evaluate deterioration process of rc structures. *Journal of Advanced Concrete Technology*, vol. 4, no. 1, pp. 147–158.

Nefovska-Danilovic, M.; Petronijevic, M. (2015):   In-plane free vibration and response analysis of isotropic rectangular plates using the dynamic stiffness method. *Computers & Structures*, vol. 152, pp. 82–95.

Nefovska-Danilovic, M.; Petronijevic, M.; Šavija, B. (2013):   Traffic-induced vibrations of frame structures. *Canadian Journal of Civil Engineering*, vol. 40, no. 2, pp. 158–171.

Pacheco, J.; Šavija, B.; Schlangen, E.; Polder, R. B. (2014):   Assessment of cracks in reinforced concrete by means of electrical resistance and image analysis. *Construction and Building Materials*, vol. 65, pp. 417–426.

Salawu, O. (1997):   Detection of structural damage through changes in frequency: a review. *Engineering Structures*, vol. 19, no. 9, pp. 718–723.

Šavija, B.; Liu, D.; Smith, G.; Hallam, K.; Schlangen, E.; Flewitt, P. (2016):   Experimentally informed multi-scale modelling of mechanical properties of quasi-brittle nuclear graphite. *Engineering Fracture Mechanics*, vol. Accepted for publication.

Šavija, B.; Luković, M.; Schlangen, E. (2014):   Lattice modeling of rapid chloride migration in concrete. *Cement and Concrete Research*, vol. 61, pp. 49–63.

Šavija, B.; Pacheco, J.; Schlangen, E. (2013):   Lattice modeling of chloride diffusion in sound and cracked concrete. *Cement and Concrete Composites*, vol. 42, pp. 30–40.

Schlangen, E.; Garboczi, E. (1997):   Fracture simulations of concrete using lattice models: computational aspects. *Engineering fracture mechanics*, vol. 57, no. 2, pp. 319–332.

Schlangen, E.; Qian, Z. (2009):   3d modeling of fracture in cement-based materials. *Journal of Multiscale Modelling*, vol. 1, no. 02, pp. 245–261.

Schlangen, E.; van Mier, J. (1992):   Simple lattice model for numerical simulation of fracture of concrete materials and structures. *Materials and Structures*, vol. 25, no. 9, pp. 534–542.

Tziviloglou, E.; Van Tittelboom, K.; Palin, D.; Wang, J.; Sierra-Beltrán, M. G.; Erşan, Y. Ç.; Mors, R.; Wiktor, V.; Jonkers, H. M.; Schlangen, E. et al. (2016): Bio-based self-healing concrete: From research to field application. *Advances in Polymer Science*.

Vasic, S.; Smith, I.; Landis, E. (2005): Finite element techniques and models for wood fracture mechanics. *Wood science and technology*, vol. 39, no. 1, pp. 3–17.

Wang, L.; Ueda, T. (2011): Mesoscale modelling of the chloride diffusion in cracks and cracked concrete. *Journal of Advanced Concrete Technology*, vol. 9, no. 3, pp. 241–249.

Wu, Z.-J.; Li, F.-M.; Zhang, C. (2014): Vibration properties of piezoelectric square lattice structures. *Mechanics Research Communications*, vol. 62, pp. 123–131.

Zienkiewicz, O. C.; Taylor, R. L. (2000): *The finite element method: Solid mechanics*, volume 2. Butterworth-heinemann.